Nano Res (2009) 2: 69–77
DOI 10.1007/s12274-009-9006-y
Research Article

Isolation of Single-Walled Carbon Nanotube Enantiomers by Density Differentiation

Alexander A. Green, Matthew C. Duch, and Mark C. Hersam (✉)

Department of Materials Science and Engineering and Department of Chemistry, Northwestern University, Evanston, Illinois 60208-3108, USA

Received: 24 October 2008 / Revised: 26 November 2008 / Accepted: 26 November 2008

ABSTRACT

Current methods of synthesizing single-walled carbon nanotubes (SWNTs) result in racemic mixtures that have impeded the study of left- and right-handed SWNTs. Here we present a method of isolating different SWNT enantiomers using density gradient ultracentrifugation. Enantiomer separation is enabled by the chiral surfactant sodium cholate, which discriminates between left- and right-handed SWNTs and thus induces subtle differences in their buoyant densities. This sorting strategy can be employed for simultaneous enrichment by handedness and roll-up vector of SWNTs having diameters ranging from 0.7 to 1.5 nm. In addition, circular dichroism of enantiomer refined samples enables identification of high-energy optical transitions in SWNTs.

KEYWORDS

Carbon nanotube, separation, handedness, enantiomer, optical activity, chirality

Chirality is a fundamental property in biology and chemistry that applies to any molecule whose mirror image cannot be superimposed on itself. Chiral molecules can exist in one of two forms known as enantiomers that are often referred to as left- or right-handed isomers. The complex interactions between biological building blocks such as amino acids and sugars require that only a single enantiomer of each molecule is present in biological systems. For synthetic molecules, however, chiral molecules are typically produced in racemic mixtures in which there are equal numbers of left- and right-handed species.

Single-walled carbon nanotubes (SWNTs), a class of one-dimensional nanomaterials with outstanding physical properties [1, 2], are a prime example of chiral molecules produced with a racemic mixture of enantiomers. SWNTs possess a unique structure which can be visualized by curling a graphene sheet into a seamless cylinder and geometrically defined by a roll-up vector (n, m) that describes its diameter and twist [3]. In this picture, one can consider left- and right-handed SWNTs to differ only by which side of the graphene sheet is curled inwards to form the cylinder. A great deal of effort has been devoted to separating SWNTs according to their roll-up vectors [4–9], as this parameter determines the SWNT electronic type (metallic or semiconducting) and the band gap of semiconducting SWNTs. It is only recently that researchers have turned their attention to isolating left- and right-handed SWNT enantiomers possessing the same roll-up vector.

Address correspondence to m-hersam@northwestern.edu

Despite the significant demands on molecular recognition required for enantiomer separation, SWNT samples enriched in a given handedness should prove useful in many areas. For instance, they exhibit optical activity that can be tuned as a function of their atomic structure [10, 11]. Furthermore, they can be employed to sense chiral molecules [12] and to study novel physical effects that are manifested in chiral one-dimensional structures [13, 14].

In previous work on enantiomer separation [15–17], Peng et al. synthesized chiral diporphyrin "nanotweezers" whose enantiomers displayed increased affinity for either left- or right-handed SWNTs. When a racemic mixture of SWNTs was sonicated in the presence of these diporphyrins and then centrifuged, the resulting supernatant was enriched in either left- or right-handed SWNTs depending on the diporphyrin enantiomer used. Peng and coworkers confirmed the success of their enrichment strategy by characterizing the optical absorbance and circular dichroism (CD) of the SWNTs. These measurements demonstrated that excitonic transitions associated with absorption peaks in the SWNTs also result in a CD signal whose sign depends on the dominant SWNT handedness.

In this article, we present an alternative strategy for isolating SWNTs of a given handedness. Like Peng et al., we use a chiral dispersion agent to encapsulate the SWNTs; however, our approach does not rely on variations in dispersion efficiency, but instead utilizes variations in the buoyant density of left- and right-handed SWNT enantiomers. These buoyant density variations are exploited using a technique known as density gradient ultracentrifugation (DGU) [18], which has previously been used to separate carbon nanotubes as a function of diameter [19], electronic type [8, 20], number of walls [21], and length [22, 23]. This DGU-based strategy offers several advantages over the previous diporphyrin work. First, it can simultaneously sort SWNTs by roll-up vector and handedness using the same dispersion agent, enabling the isolation of multiple highly pure, enantiomer refined samples in a single experiment. Second, it can be used for enantiomer enrichment of SWNTs with diameters ranging from 0.7 to 1.5 nm, in contrast to previous work that has been limited to SWNTs with diameters less than 1.0 nm. Third, the reagents used in DGU do not require custom chemical synthesis and are readily available commercially.

Enantiomer separation is achieved using SWNTs encapsulated by the chiral surfactant sodium cholate (SC). SC possesses a rigid, planar structure (Fig. 1(a)) with opposing hydrophobic and hydrophilic faces [24] that can associate with the SWNT sidewalls and surrounding water molecules, respectively. Previous ultracentrifugation experiments [8, 25] have indicated that SC possesses strong molecular recognition characteristics and coats SWNTs in an ordered, reproducible manner. This reliable SC encapsulation produces SWNT-SC complexes with buoyant densities that are strongly related to the SWNT diameter. In addition, the chiral structure of SC is expected to encapsulate left- and right-handed SWNTs differently (Fig. 1(c)), resulting in SC-SWNT enantiomer complexes with slightly different buoyant densities.

DGU enantiomer separation was conducted using CoMoCAT SWNTs dispersed in 1% w/v

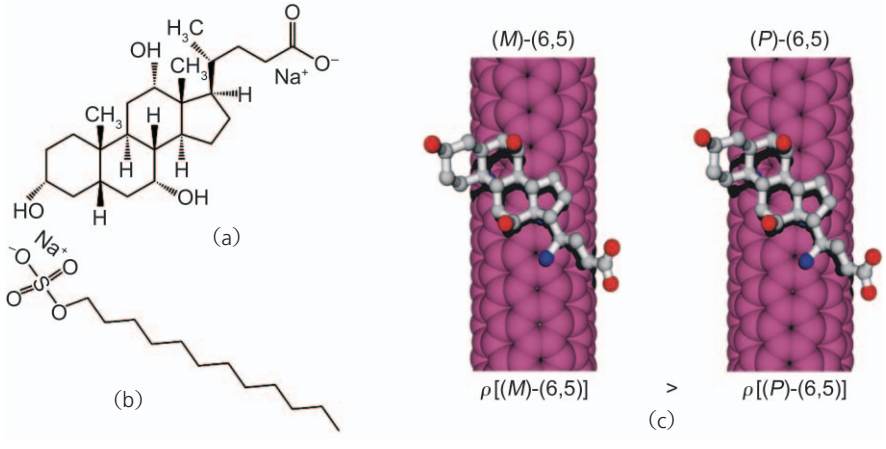

Figure 1 (a) Chemical structure of the chiral sodium cholate surfactant; (b) chemical structure of the achiral sodium dodecyl sulfate surfactant; (c) schematic illustration of the interaction of chiral left-handed (*M*) and right-handed (*P*) (6,5)-SWNTs with sodium cholate, which causes small differences in the buoyant density, ρ, of SWNT enantiomers. For the sodium cholate molecule, carbon atoms, methyl groups, and oxygen atoms are represented as gray, blue, and red spheres, respectively

SC aqueous solution (see Methods). The SWNT dispersion was concentrated, added to a linear density gradient, and then centrifuged at a maximum centripetal acceleration of 288 000 g for 12 h (see Methods). Following ultracentrifugation, the bright, colored bands of separated SWNTs (Fig. 2(a)) were removed from the centrifuge tube in 0.25 mm (~35 μL) fractions and characterized using visible/near infrared spectroscopy and CD. Figure 2(b) presents the optical absorbance spectra of several of the sorted fractions. In the most buoyant fractions, the small diameter (6,4)-SWNTs (0.69 nm diameter) are enriched as evidenced by the peak at 881 nm in fraction f15 corresponding to the E_{11}^{S} transition of these SWNTs. In subsequent fractions, (7,3)-SWNTs (0.70 nm diameter), (6,5)-SWNTs (0.76 nm diameter), and (7,5)-SWNTs (0.83 nm diameter) are enriched at progressively higher densities. The CD from the SWNTs (Fig. 2(c)) contains a significant background signal that is most likely caused by residual SC that cannot be completely removed by subtracting the CD signal of a 1% w/v SC reference solution. Despite this background contribution, unambiguous CD peaks are observed in the spectra of all the sorted fractions while the CD signal from the unsorted CoMoCAT SWNTs does not possess such features. Most of the optical activity observed in the 500 to 700 nm wavelength range can be assigned to the E_{22}^{S} transitions of (6,4)-, (6,5)-, and (7,5)-SWNTs, and corresponds to the peaks observed in the absorbance spectra.

Several strong CD peaks, however, are not correlated to comparatively strong absorbance peaks. For fraction f18 in Figs. 2(b) and 2(c), there is a strong CD transition at ~640 nm that displays only weak absorbance and corresponds to the E_{12}^{S} transition of the (6,5)-SWNT [26, 27]. Although this E_{12}^{S} excitation overlaps closely with the E_{22}^{S} transition of (7,5)-SWNTs, its CD intensity follows closely the behavior of the E_{22}^{S} CD transition of (6,5)-SWNTs over multiple sorted SWNT fractions. In addition, CD peaks in the 400 to 500 nm range are not well correlated with the E_{11}^{M} absorption peaks observed for metallic SWNTs in this region (see Fig. S-1 in the Electronic Supplementary Material (ESM)). We attribute these uncorrelated CD peaks to E_{13}^{S} and E_{31}^{S} transitions arising from transverse SWNT excitations (discussed in more detail below). While the absorption strength of these transverse E_{12}^{S}, E_{13}^{S}, and E_{31}^{S} transitions is significantly weaker than that of longitudinal excitations such as E_{22}^{S} and E_{11}^{M} [26, 28, 29], theoretical work has predicted that transverse excitations should exhibit stronger optical activity

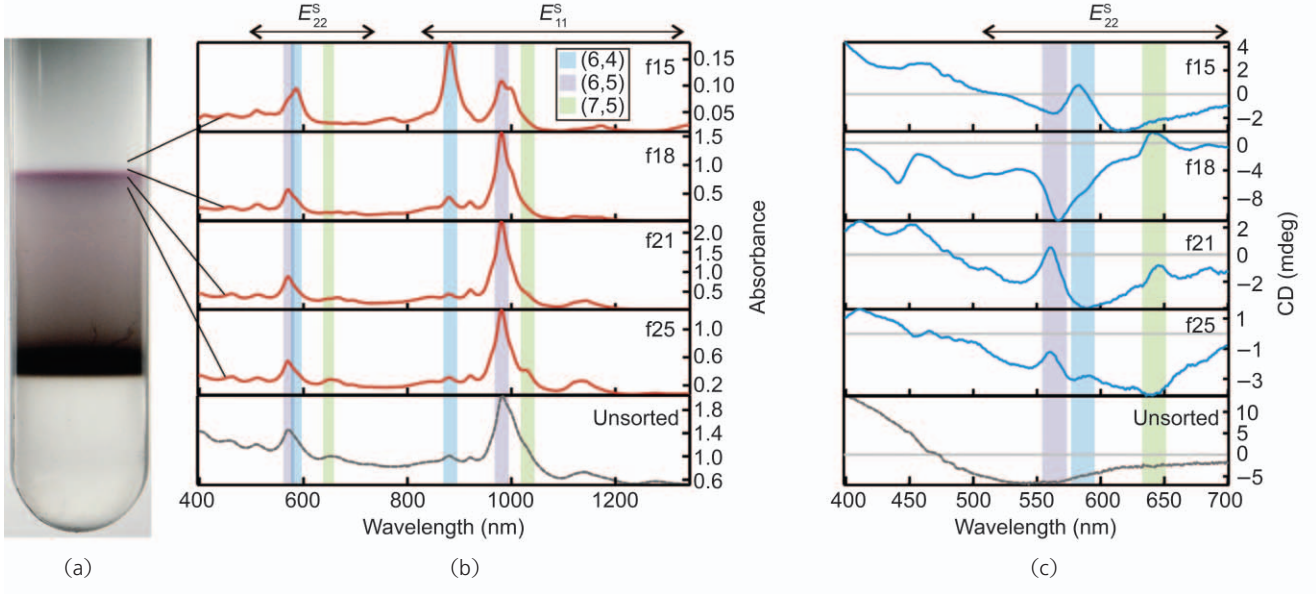

Figure 2 (a) Photograph of a centrifuge tube following enantiomer enrichment of CoMoCAT SWNTs. (b) Visible/near infrared absorbance spectra of CoMoCAT SWNTs following density gradient ultracentrifugation. The SWNT fractions (f15, f18, f21, and f25) were collected at positions marked with black lines on the centrifuge tube. The absorbance spectrum of the unsorted SWNTs is presented in the lowest curve (dashed, gray). (c) CD spectra of the sorted SWNT fractions (f15, f21, f21, and f25) and unsorted CoMoCAT SWNTs (dashed, gray)

than longitudinal ones [10], which could explain their comparatively strong CD intensity.

To gain further insight into DGU-based enantiomer sorting, the absorbance and CD spectra from multiple fractions were analyzed to extract the relative concentrations of SWNTs of a given handedness and roll-up vector as a function of buoyant density (see Methods). Following the data provided in Ref. [16], all SWNTs having a positive E_{22}^{S} transition CD peak were identified as left-handed and denoted (*M*) in the IUPAC nomenclature [30], while those SWNTs with a negative E_{22}^{S} transition CD peak were identified as right-handed and denoted (*P*). The optical absorbance analysis indicates that SWNTs with (6,4), (6,5), and (7,5) roll-up vectors possess mean buoyant densities that fall within 10 mg/cm^3 (Fig. 3(a)), yet their buoyant density distributions exhibit full width at half maximum values of comparable magnitude – a factor that limits the degree of refinement afforded by DGU. Previously, the broadening of the SWNT buoyant density distributions was attributed to diffusion, variations in surfactant encapsulation, mixing during fractionation, and SWNT defects [8]. Analysis of the CD spectra presented in Figs. 3(b) and 3(c), however, suggests that handedness effects contribute significantly to this broadening. In particular, the mean buoyant densities of left- and right-handed enantiomers of SWNTs with a given roll-up vector differ from each other and the mean buoyant density of the (*n*,*m*)-SWNTs overall (Fig. 3(a)). Moreover, the buoyant density distributions of the SWNT enantiomers are somewhat sharper than the corresponding (*n*,*m*)-SWNT distribution. The CD results also indicate that SC does not have a consistent affinity for a particular SWNT handedness for all roll-up vectors, which implies that the SWNT enantiomer possessing the lower buoyant density when complexed with SC must depend on the SWNT roll-up vector and diameter. Enantiomer separation was also observed for SWNTs having (7,3), (9,1), and (8,3) roll-up vectors. However, the CD signals of these nanotubes were weaker than those of (6,4), (6,5), and (7,5) species, which suggests that SC encapsulation may have greater sensitivity to SWNTs with larger roll-up angles.

For further optical characterization, we dialyzed the sorted SWNT dispersions into 1% w/v sodium dodecyl sulfate (SDS) solution. This processing step eliminates the CD contribution from the chiral SC molecules and reveals higher energy SWNT optical transitions that are obscured by the density gradient medium iodixanol. In addition, dialysis ensures that any CD induced by interactions between SC and the

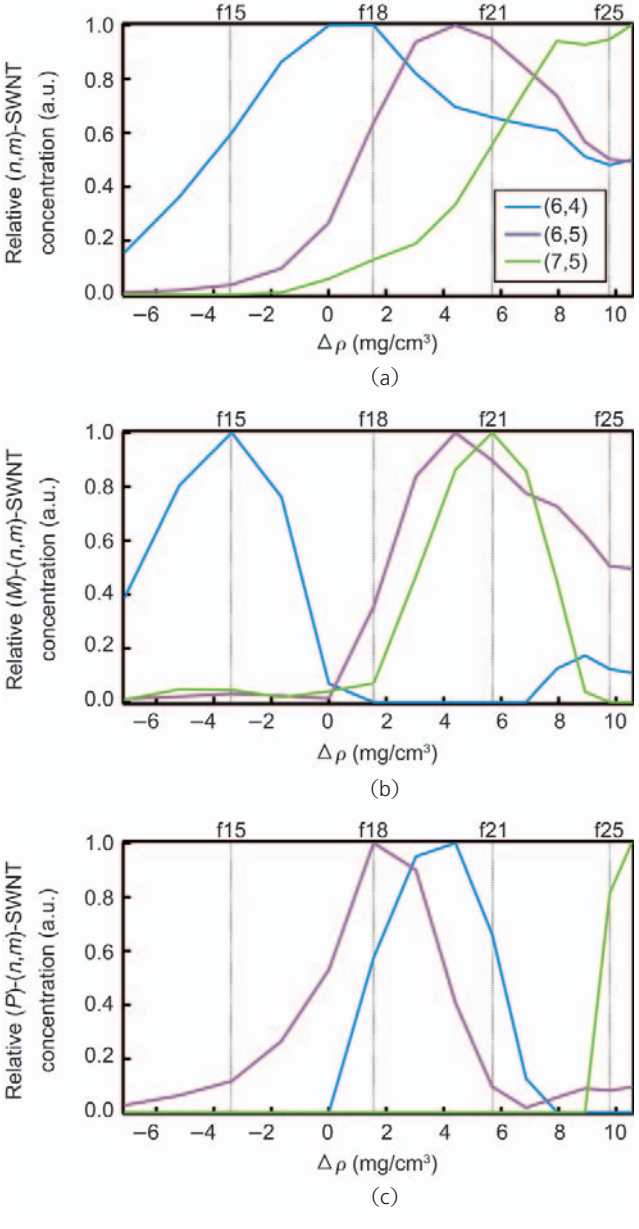

Figure 3 The relative SWNT concentration for (a) (*n*,*m*)-SWNTs overall, (b) (*M*)-(*n*,*m*)-SWNTs, and (c) (*P*)-(*n*,*m*)-SWNTs as a function of SWNT buoyant density. The SWNT buoyant density is referenced to 1.08 g/cm^3 ± 0.01 g/cm^3 where $\Delta\rho = 0$ g/cm^3. The buoyant densities of the sorted CoMoCAT fractions characterized in Fig. 2 are marked by dotted gray lines

SWNTs [31] can be eliminated following replacement by the achiral SDS molecule (Fig. 1(b)). Optical absorbance and CD spectra from these dialyzed samples are presented in Fig. 4. To better compare CD intensity, the absorbance of the dominant E^S_{22} transition is normalized to unity and the CD spectra are scaled accordingly. The fraction enriched in (*M*)-(6,4)-SWNTs exhibits the strongest CD signal with a magnitude exceeding 60 mdeg (Fig. 4(a)). For the two denser fractions (Fig. 4(b)), the CD signal decreases as contributions from bundled SWNTs with higher buoyant densities become more prevalent, thus obscuring the CD from isolated SWNTs.

In agreement with theory [11] and previous results [16], the CD signal alternates in sign as the order of the transitions increases (E^S_{22} , E^S_{33} , and E^S_{44}) for the (6,5)-SWNT enantiomers, with (*P*)-(6,5)-SWNTs following a (−,+,−) progression and (*M*)-(6,5)-SWNTs displaying the inverted (+,−,+) pattern (Fig. 4(b)). The E^S_{44} transitions, previously not observed in enantiomer separated samples, exhibit significantly weaker CD than the E^S_{33} transitions and appear to end the trend of increasing CD intensity with transition order reported for the E^S_{11} , E^S_{22} , and E^S_{33} excitations [16]. The (*M*)-(6,4)-SWNTs, in contrast, do not display a pattern of alternating CD signs with increasing energy, instead following a (+,+,−) sequence (Fig. 4(a)). Furthermore, the magnitude of the CD signal increases monotonically with energy, instead of displaying the expected attenuation for the highest energy transition. This behavior can be attributed to the energy crossover for the E^S_{33} and E^S_{44} excitonic transitions previously reported for (6,4)-SWNTs in the literature [32].

The reduction in background CD signal after sample dialysis also allows a more transparent analysis of the optically active excitations attributed to the E^S_{12} , E^S_{13} , and E^S_{31} cross-polarized transitions. Following dialysis, these transverse excitations continue to display strong CD intensity and relatively weak absorbance. The E^S_{21} transition is most evident in the spectra from the (*P*)-(6,5)-SWNTs and occurs at 638 nm, in agreement with results presented in Refs. [26, 27]. However, the transition previously observed at ~605 nm [26] could not be clearly resolved as a result of its proximity to the (6,4)-SWNT E^S_{22} excitation. The strong CD feature at 440 nm in the (*P*)- and (*M*)-(6,5)-SWNTs is assigned to the E^S_{13} transition,

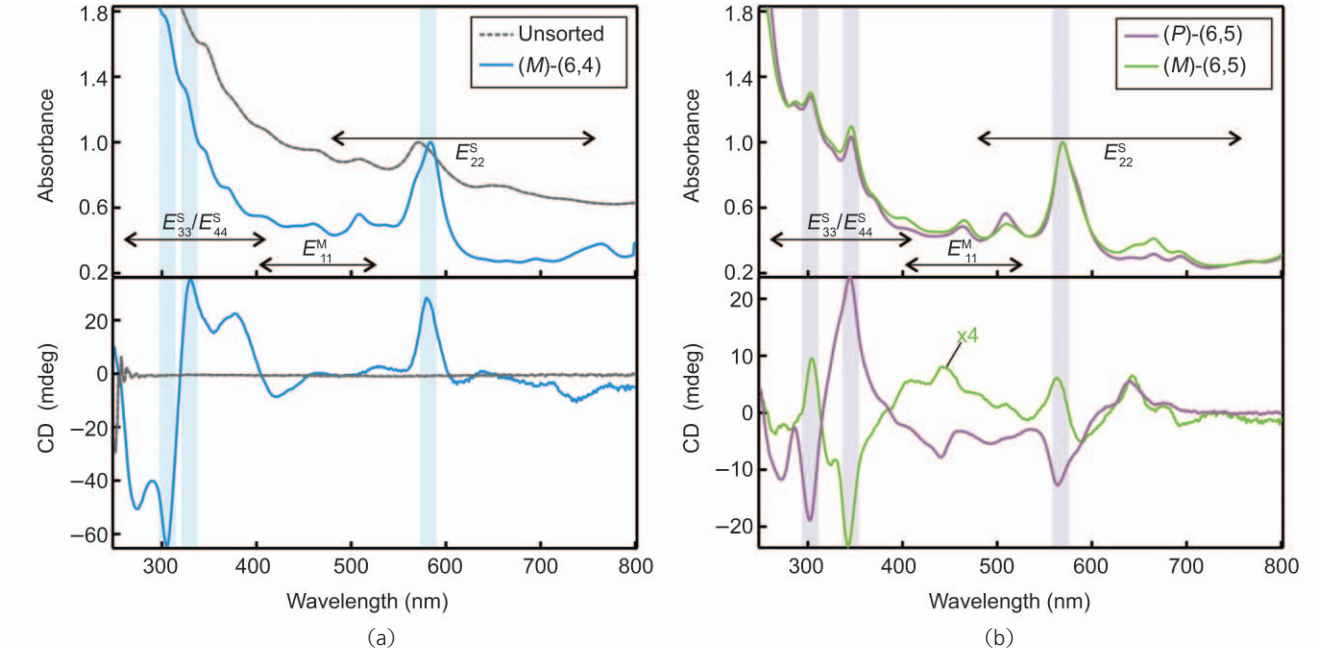

Figure 4 Optical absorbance and CD spectra following dialysis into 1% w/v SDS aqueous solution of (a) unsorted CoMoCAT SWNTs and (*M*)-(6,4)-SWNTs from f15, and (b) (*P*)-(6,5)-SWNTs and (*M*)-(6,5)-SWNTs from f18 and f21, respectively. E^S_{22} , E^S_{33} , and E^S_{44} excitonic transitions of the (6,4)-SWNTs and (6,5)-SWNTs are shaded in (a) and (b), respectively. The optical absorbance spectrum of each sample is scaled by setting the intensity of the strongest E^S_{22} transition to unity with the corresponding CD spectrum also modified by the same scaling factor

while the shoulder observed at 424 nm in (*P*)-(6,5)-SWNTs may be due to the E^S_{31} transition.

Since both E^S_{13} and E^S_{31} excitations of (6,5)-SWNTs to our knowledge have not been reported elsewhere, additional analysis and measurements were taken to ensure these CD features did not arise from metallic SWNTs or large diameter semiconducting SWNTs. By superimposing the absorbance and CD spectra from (*P*)- and (*M*)-(6,5)-SWNTs, the spectral features from these measurements can be directly compared (see Fig. S-2 in the ESM). A strong optical absorbance peak assigned to (6,6) and (7,4) SWNTs [33] is located at 460 nm; however, the E^S_{13} CD peak occurs at 440 nm where the SWNT absorbance is free of any transitions. In addition, the photoluminescence from the sorted SWNT solutions was measured at an excitation wavelength of 440 nm and did not reveal any emission from SWNTs with diameters larger than 0.9 nm whose E^S_{33} transitions should have been excited if present. The assignment of the features to E^S_{13} and E^S_{31} transverse excitations is further supported by the opposite signs of their CD signal for the two (6,5)-SWNT enantiomers, which is consistent with the behavior observed for the longitudinal excitations.

The energies of the E^S_{13} and E^S_{31} transitions are also found to follow trends observed for E^S_{12} and E^S_{21} transitions. In the tight binding model, the energies of the cross-polarized E^S_{12} and E^S_{13} excitations are expected to lie at approximately $(E^S_{11} + E^S_{22})/2$ and $(E^S_{11} + E^S_{33})/2$, respectively, with the E^S_{21} and E^S_{31} transitions located at slightly different energies as a result of electron-hole asymmetry [34]. However, several previous reports [26–28] have shown the E^S_{12} energies are blue-shifted by ~200 meV from $(E^S_{11} + E^S_{33})/2$ as a result of Coulomb interactions [35, 36]. Here, the experimentally observed E^S_{13} and E^S_{31} transitions were found to be blue-shifted by 380 meV and 490 meV from $(E^S_{11} + E^S_{33})/2$, respectively. This shift corresponds to 19% of the energy difference between the E^S_{11} and E^S_{33} , which is comparable to the blue-shift of 23% measured for the E^S_{12} excitation compared to E^S_{22}–E^S_{11}.

To demonstrate the generality of DGU-based enantiomer enrichment, separations were also carried out for arc discharge grown SWNTs with an average diameter of 1.4 nm (see Methods). Following dialysis into 1% w/v SDS, the sorted SWNT fractions exhibit noticeable changes in their optical absorbance peaks indicative of roll-up vector sorting and strong CD signals characteristic of successful enantiomer separation (Fig. 5). In contrast, the unsorted SWNTs display no detectable optical activity. The SWNTs in fraction g8 present clear indications of metallic SWNT enantiomer enrichment with peaks in absorbance at 740 nm (E^M_{11}) and from 415 to 440 nm (E^M_{22}) being complemented by strong negative and positive CD peaks, respectively. Based on the E^M_{11} transition wavelength of these SWNTs [20], their diameters are estimated to be ~1.5 nm. Complementary absorption and CD signals are also observed for semiconducting SWNTs in the arc discharge samples. However, the number of possible SWNTs and overlapping SWNT transition energies in the 1.4 nm diameter range make assignment of roll-up vectors ambiguous.

In conclusion, we have described an enantiomer separation method using SWNTs encapsulated by the chiral surfactant SC. Sorting is effectuated by small variations in the ordering of SC around left- and right-handed SWNTs, which induces changes in buoyant density that are exploited using DGU. This

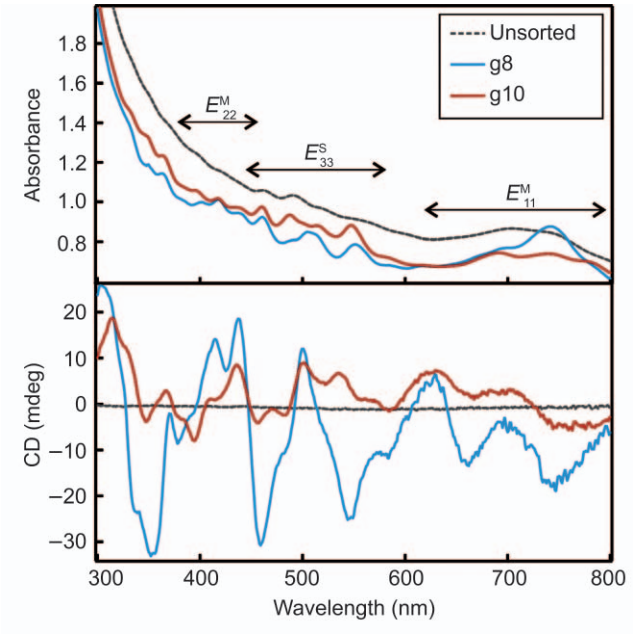

Figure 5 Optical absorbance and CD spectra of unsorted and enantiomer enriched arc discharge SWNTs following dialysis into 1% w/v SDS aqueous solution. The optical absorbance spectrum of each sample is scaled by setting the intensity of the strongest E^S_{22} transition to unity with the corresponding CD spectrum also modified by the same scaling factor

approach can be used for enantiomer separation of SWNTs with diameters ranging from 0.7 to 1.5 nm. The highly refined SWNT enantiomers resulting from these separations exhibit strong optical activity and provide valuable information concerning the physical properties of SWNTs. For example, transverse SWNT excitations not easily detected in as-produced samples can be observed in the CD spectra of enantiomer enriched samples. Furthermore, the polarity and magnitude of CD signals arising from the refined samples can be used for the assignment of higher lying excitonic transitions, including those whose energies cross over. Since DGU is scaleable and iteratively repeatable, this work serves as the foundation for large-scale production of high purity enantiomer-refined SWNTs.

Methods

Dispersion of SWNTs by ultrasonication. CoMoCAT SWNTs (Southwest Nanotechnologies, Inc.) were added to 60 mL of 1% w/v SC aqueous solution at a loading of ~1 mg/mL. The mixture was then horn ultrasonicated (Fisher Scientific Model 500 Sonic Dismembrator) for 40 min using a 13 mm diameter tip operating at 40% of its maximum amplitude. The arc discharge SWNTs (Carbon Solutions, Inc.) were dispersed in a volume of 110 mL of 1% w/v SC with SWNT loading of ~1.5 mg/mL. This mixture was also ultrasonicated at 40% amplitude for 40 min using a 13 mm diameter tip.

Enantiomer enrichment of SWNTs using DGU and optical characterization. CoMoCAT SWNTs were sorted by handedness in a density gradient with a surfactant loading of 1% w/v SC throughout. Starting from the bottom of the centrifuge tube, the gradient had the following structure: 1.5 mL, 60% w/v iodixanol underlayer; 5 mL, 30% to 15% w/v iodixanol linear gradient; 1 mL, 12.5% w/v iodixanol CoMoCAT SWNT layer; and a ~4.5 mL, 0% w/v iodixanol overlayer. The layered tube was then centrifuged in an SW41 Ti rotor (Beckman Coulter, Inc.) for 12 h at 41 000 rpm and 22 °C. Following ultracentrifugation, sorted SWNTs were recovered using a piston gradient fractionator (Biocomp Instruments, Inc.) which collected 0.25 mm fractions. Enantiomer enrichment of arc discharge SWNTs (Carbon Solutions, Inc.) was also carried out in density gradients loaded with 1% w/v SC throughout. The centrifuge tube was layered from bottom to top with the following components: 1.5 mL, 60% w/v iodixanol underlayer; 5 mL, 37.5% to 22.5% w/v iodixanol linear gradient; 0.88 mL, 35% w/v iodixanol SWNT layer; and a ~4.6 mL, 0% w/v iodixanol overlayer. Fractions 0.5 mm in height were collected using a piston gradient fractionator following ultracentrifugation in an SW41 Ti rotor for 12 h at 41 000 rpm and 22 °C. All optical absorbance measurements were carried out using a Varian Cary 500 spectrophotometer, and CD spectra were obtained using a Jasco J-715 CD spectrometer.

Analysis of optical absorbance and CD spectra. Optical absorbance and CD spectra were analyzed using a least squares fitting algorithm. The spectra were fitted to a set of Lorentzian lineshapes and polynomial functions in energy that represented distinct (n,m) SWNT species and the background signal, respectively. The energies of the SWNT transitions were taken from Ref. [37] and red-shifted to account for the dielectric constant of SC. For the absorbance spectra, both the E_{11}^{S} and E_{22}^{S} transitions were fitted over the wavelength range of 480–1340 nm and the E_{22}^{S} peak amplitude was set to a quarter of the E_{11}^{S} peak amplitude. For the CD spectra, fitting was applied only to the E_{22}^{S} region of 500–700 nm. Based on the experimental data, the E_{22}^{S} transition energies of (M)-SWNTs were blue-shifted by ~20 meV compared to (P)-SWNTs, which facilitated deconvolution of the contributions from left- and right-handed species using separate basis functions. This blue-shift appears to be related to SC-encapsulation and was not present following dialysis into the achiral SDS surfactant. The E_{12}^{S} transition of the (6,5)-SWNTs at ~640 nm also had to be taken into account given its proximity to the E_{22}^{S} of (7,5)-SWNTs. The (6,5)-SWNT E_{12}^{S} transition [26, 27] had the opposite sign of the (6,5)-SWNT E_{22}^{S} peak and was set to 57% of the E_{22}^{S} amplitude to produce the best agreement with the experimental data.

In order to generate the curves in Fig. 3, the fitting coefficients representing the concentration of each SWNT species were first extracted from the least squares algorithm. The coefficients for a given (n,m)

–SWNT in absorbance or (*M*)-/(*P*)-(*n*,*m*)-SWNT in CD were then normalized by setting to unity the maximum value of the coefficients over the series of 14 fractions to produce relative concentration values. The (6,4)-, (6,5)-, and (7,5)-SWNTs presented the greatest degree of enantiomer enrichment and their relative concentration profiles are displayed in Fig. 3. Weak enantiomer refinement was also observed for (7,3)-, (9,1)-, and (8,3)-SWNTs.

Acknowledgements

The authors thank M. S. Arnold for helpful discussions and preliminary measurements. This work was supported by the U.S. Army Telemedicine and Advanced Technology Research Center (DAMD17-05-1-0381) and the National Science Foundation (DMR-0520513, EEC-0647560, and DMR-0706067). A Natural Sciences and Engineering Research Council of Canada Postgraduate Scholarship (A. A. Green) and an Alfred P. Sloan Research Fellowship (M. C. Hersam) are also acknowledged. This work made use of instruments in the Keck-II facility of the NUANCE Center and the Keck Biophysics Facility at Northwestern University. The NUANCE Center is supported by NSF-NSEC, NSF-MRSEC, Keck Foundation, the State of Illinois, and Northwestern University.

Electronic Supplementary Material: Supplementary material is available in the online version of this article at http://dx.doi.org/10.1007/s12274-009-9006-y and is accessible free of charge.

References

[1] Javey, A.; Guo, J.; Wang, Q.; Lundstrom, M.; Dai, H. J. Ballistic carbon nanotube field-effect transistors. *Nature* **2003**, *424*, 654–657.

[2] Yu, M. F.; Lourie, O.; Dyer, M. J.; Moloni, K.; Kelly, T. F.; Ruoff, R. S. Strength and breaking mechanism of multiwalled carbon nanotubes under tensile load. *Science* **2000**, *287*, 637–640.

[3] Hu, J. T.; Odom, T. W.; Lieber, C. M. Chemistry and physics in one dimension: Synthesis and properties of nanowires and nanotubes. *Acc. Chem. Res.* **1999**, *32*, 435–445.

[4] Hersam, M. C. Progress towards monodisperse single-walled carbon nanotubes. *Nature Nanotech.* **2008**, *3*, 387–394.

[5] Krupke, R.; Hennrich, F.; von Lohneysen, H.; Kappes, M. M. Separation of metallic from semiconducting single-walled carbon nanotubes. *Science* **2003**, *301*, 344–347.

[6] Zheng, M.; Jagota, A.; Strano, M. S.; Santos, A. P.; Barone, P.; Chou, S. G.; Diner, B. A.; Dresselhaus, M. S.; McLean, R. S.; Onoa, G. B.; Samsonidze, G. G.; Semke, E. D.; Usrey, M.; Walls, D. J. Structure-based carbon nanotube sorting by sequence-dependent DNA assembly. *Science* **2003**, *302*, 1545–1548.

[7] Chattopadhyay, D.; Galeska, L.; Papadimitrakopoulos, F. A route for bulk separation of semiconducting from metallic single-wall carbon nanotubes. *J. Am. Chem. Soc.* **2003**, *125*, 3370–3375.

[8] Arnold, M. S.; Green, A. A.; Hulvat, J. F.; Stupp, S. I.; Hersam, M. C. Sorting carbon nanotubes by electronic structure using density differentiation. *Nature Nanotech.* **2006**, *1*, 60–65.

[9] Nish, A.; Hwang, J. Y.; Doig, J.; Nicholas, R. J. Highly selective dispersion of singlewalled carbon nanotubes using aromatic polymers. *Nature Nanotech.* **2007**, *2*, 640–646.

[10] Samsonidze, G. G.; Gruneis, A.; Saito, R.; Jorio, A.; Souza, A. G.; Dresselhaus, G.; Dresselhaus, M. S. Interband optical transitions in left- and right-handed single-wall carbon nanotubes. *Phys. Rev. B* **2004**, *69*, 205402.

[11] Tasaki, S.; Maekawa, K.; Yamabe, T. π-band contribution to the optical properties of carbon nanotubes: Effects of chirality. *Phys. Rev. B* **1998**, *57*, 9301–9318.

[12] Vardanega, D.; Picaud, F.; Girardet, C. Chiral response of single walled carbon nanotube-based sensors to adsorption of amino acids: A theoretical model. *J. Chem. Phys.* **2007**, *127*, 194702.

[13] Strano, M. S. Carbon nanotubes—Sorting out left from right. *Nature Nanotech.* **2007**, *2*, 340–341.

[14] Ivchenko, E. L.; Spivak, B. Chirality effects in carbon nanotubes. *Phys. Rev. B* **2002**, *66*, 155404.

[15] Peng, X.; Komatsu, N.; Bhattacharya, S.; Shimawaki, T.; Aonuma, S.; Kimura, T.; Osuka, A. Optically active single-walled carbon nanotubes. *Nature Nanotech.* **2007**, *2*, 361–365.

[16] Peng, X. B.; Komatsu, N.; Kimura, T.; Osuka, A. Improved

optical enrichment of SWNTs through extraction with chiral nanotweezers of 2,6-pyridylene-bridged diporphyrins. *J. Am. Chem. Soc.* **2007**, *129*, 15947–15953.

[17] Peng, X.; Komatsu, N.; Kimura, T.; Osuka, A. Simultaneous enrichments of optical purity and (*n*,*m*) abundance of SWNTs through extraction with 3,6-carbazolylene-bridged chiral diporphyrin nanotweezers. *ACS Nano* **2008**, *2*, 2045–2050.

[18] Green, A. A.; Hersam, M. C. Ultracentrifugation of single-walled nanotubes. *Mater. Today* **2007**, *10*, 59–60.

[19] Arnold, M. S.; Stupp, S. I.; Hersam, M. C. Enrichment of single-walled carbon nanotubes by diameter in density gradients. *Nano Lett.* **2005**, *5*, 713–718.

[20] Green, A. A.; Hersam, M. C. Colored semitransparent conductive coatings consisting of monodisperse metallic single-walled carbon nanotubes. *Nano Lett.* **2008**, *8*, 1417–1422.

[21] Green, A. A.; Hersam, M. C. Processing and properties of highly enriched double-walled carbon nanotubes. *Nature Nanotech.*, in press **2009**. (DOI:10.1038/nnano.2008.364).

[22] Sun, X.; Zaric, S.; Daranciang, D.; Welsher, K.; Lu, Y.; Li, X.; Dai, H. Optical properties of ultrashort semiconducting single-walled carbon nanotube capsules down to sub-10 nm. *J. Am. Chem. Soc.* **2008**, *130*, 6551–6555.

[23] Fagan, J. A.; Becker, M. L.; Chun, J.; Hobbie, E. K. Length fractionation of carbon nanotubes using centrifugation. *Adv. Mater.* **2008**, *20*, 1609–1614.

[24] Mukhopadhyay, S.; Maitra, U. Chemistry and biology of bile acids. *Curr. Sci.* **2004**, *87*, 1666–1683.

[25] Arnold, M. S.; Suntivich, J.; Stupp, S. I.; Hersam, M. C. Hydrodynamic characterization of surfactant encapsulated carbon nanotubes using an analytical ultracentrifuge. *ACS Nano* **2008**, *2*, 2291–2300.

[26] Miyauchi, Y.; Oba, M.; Maruyama, S. Cross-polarized optical absorption of single-walled nanotubes by polarized photoluminescence excitation spectroscopy. *Phys. Rev. B* **2006**, *74*, 205440

[27] Chuang, K. C.; Nish, A.; Hwang, J. Y.; Evans, G. W.; Nicholas, R. J. Experimental study of Coulomb corrections and single-particle energies for single-walled carbon nanotubes using cross-polarized photoluminescence. *Phys. Rev. B* **2008**, *78*, 085411.

[28] Lefebvre, J.; Finnie, P. Polarized photoluminescence excitation spectroscopy of single-walled carbon nanotubes. *Phys. Rev. Lett.* **2007**, *98*, 167406.

[29] Kilina, S.; Tretiak, S.; Doorn, S. K.; Luo, Z.; Papadimitrakopoulos, F.; Piryatinski, A.; Saxena, A.; Bishop, A. R. Cross-polarized excitons in carbon nanotubes. *P. Natl. Acad. Sci. USA* **2008**, *105*, 6797–6802.

[30] Cross, L. C.; Klyne, W. Report from IUPAC commission on nomenclature of organic chemistry—Rules for nomenclature of organic chemistry. Section E: Stereochemistry (recommendations 1974). *Pure Appl. Chem.* **1976**, *45*, 13–30.

[31] Dukovic, G.; Balaz, M.; Doak, P.; Berova, N. D.; Zheng, M.; McLean, R. S.; Brus, L. E. Racemic single-walled carbon nanotubes exhibit circular dichroism when wrapped with DNA. *J. Am. Chem. Soc.* **2006**, *128*, 9004–9005.

[32] Haroz, E. H.; Bachilo, S. M.; Weisman, R. B.; Doorn, S. K. Curvature effects on the E_{33} and E_{44} exciton transitions in semiconducting single-walled carbon nanotubes. *Phys. Rev. B* **2008**, *77*, 125405.

[33] Jorio, A.; Santos, A. P.; Ribeiro, H. B.; Fantini, C.; Souza, M.; Vieira, J. P. M.; Furtado, C. A.; Jiang, J.; Saito, R.; Balzano, L.; Resasco, D. E.; Pimenta, M. A. Quantifying carbon-nanotube species with resonance Raman scattering. *Phys. Rev. B* **2005**, *72*, 075207.

[34] Gruneis, A.; Saito, R.; Jiang, J.; Samsonidze, G. G.; Pimenta, M. A.; Jorio, A.; Souza, A. G.; Dresselhaus, G.; Dresselhaus, M. S. Resonant Raman spectra of carbon nanotube bundles observed by perpendicularly polarized light. *Chem. Phys. Lett.* **2004**, *387*, 301–306.

[35] Uryu, S.; Ando, T. Exciton absorption of perpendicularly polarized light in carbon nanotubes. *Phys. Rev. B* **2006**, *74*, 155–411.

[36] Zhao, H. B.; Mazumdar, S. Electron-electron interaction effects on the optical excitations of semiconducting single-walled carbon nanotubes. *Phys. Rev. Lett.* **2004**, *93*, 157–402.

[37] Weisman, R. B.; Bachilo, S. M. Dependence of optical transition energies on structure for single-walled carbon nanotubes in aqueous suspension: An empirical Kataura plot. *Nano Lett.* **2003**, *3*, 1235–1238.